Isotopic yield measurement in the heavy mass region for ^{239}Pu thermal neutron induced fission

A. Bail,* O. Serot, L. Mathieu,† and O. Litaize
CEA, DEN-Cadarache, F-13108 Saint-Paul-lez-Durance, France

T. Materna, U. Köster, and H. Faust
Institut Laue Langevin, 6 rue Jules Horowitz, B.P. 156, F-38042, Grenoble, France

A. Letourneau and S. Panebianco
CEA, DSM-Saclay, IRFU/SPhN, F-91191 Gif-sur-Yvette, France
(Received 14 June 2011; published 6 September 2011)

Despite the huge number of fission yield data available in the different evaluated nuclear data libraries, such as JEFF-3.1.1, ENDF/B-VII.0, and JENDL-4.0, more accurate data are still needed both for nuclear energy applications and for our understanding of the fission process itself. It is within the framework of this that measurements on the recoil mass spectrometer Lohengrin (at the Institut Laue-Langevin, Grenoble, France) was undertaken, to determine isotopic yields for the heavy fission products from the ^{239}Pu(n_{th},f) reaction. In order to do this, a new experimental method based on γ-ray spectrometry was developed and validated by comparing our results with those performed in the light mass region with completely different setups. Hence, about 65 fission product yields were measured with an uncertainty that has been reduced on average by a factor of 2 compared to that previously available in the nuclear data libraries. In addition, for some fission products, a strongly deformed ionic charge distribution compared to a normal Gaussian shape was found, which was interpreted as being caused by the presence of a nanosecond isomeric state. Finally, a nuclear charge polarization has been observed in agreement, with the one described on other close fissioning systems.

DOI: 10.1103/PhysRevC.84.034605 PACS number(s): 25.85.Ec, 29.30.Aj, 29.30.Kv

I. INTRODUCTION

Nuclear fission is a very complex phenomenon resulting from collective and intrinsic excitations within the nucleus in which fine structure effects and energy dissipation play a crucial role. Owing to this complexity and despite many theoretical works, this many-body problem is not yet well understood and the main fission observables are still extremely difficult to reproduce. In particular, various models were proposed to calculate the mass yield distributions (see Ref. [1] for a detailed review of these theoretical models): a statistical model [2], a microscopic-macroscopic model [3], or even a pure microscopic model including a dynamical treatment of the fissioning nucleus [4]. Unfortunately, mass yields obtained by these different calculations are still very far from providing the accuracy required by nuclear applications.

Because fission yield data are of importance in the various nuclear energy applications (reactivity or decay heat in nuclear power, postirradiation experiments, neutron flux determination, and so on), a large number of experiments have been carried out on this field during the last decades and were generally incorporated into the main evaluated nuclear data libraries such as JEFF-3.1.1 [5], ENDF/B-VII.0 [6], and JENDL-4.0 [7]. Nevertheless, strong efforts are needed to reduce fission yield uncertainties as well as to understand differences observed between these evaluated nuclear data libraries. This is caused by more stringent radiation protection security requirements and to intentions to extend reactor life times.

Measuring isotopic fission yields is not an easy task. Most common experiments use the radiochemical techniques. Coupled with γ-ray spectroscopy, this type of experiment provides a very accurate cumulative isotopic yield but is, unfortunately, limited to only few isotopes. Another very usual method is based on the specific fission product energy loss when crossing a given material, which allows good nuclear charge identification. However, the nuclear charge resolution is good enough only in the light mass region. A nice review of the experimental procedures used for mass and/or charge yield determination os goven in Ref. [8].

At the Lohengrin recoil mass spectrometer located at the Institut Laue-Langevin in Grenoble (France), various nuclei undergoing fission in a thermal neutron flux (^{229}Th [9], ^{233}U [10], ^{235}U [11–13], ^{237}Np [14], ^{238}Np [15], ^{239}Pu [16], ^{241}Pu [17], ^{242m,g}Am [18], ^{245}Cm [19], ^{249}Cf [20]) have been investigated up to now. Detailed results for kinetic energy, mass, and nuclear charge distributions were deduced with the best precision. However, only light fission products[1] were measured (except for ^{245}Cm [19,21], for which mass yields were determined in both light and heavy regions). Indeed, combining the Lohengrin mass spectrometer with a

*bailadeline@yahoo.fr; presently at CEA, DAM-Ile de France, F-91290 Arpajon, France.
†Presently at CENBG, Chemin du Solarium, le Haut Vigneau, BP 120, F-33175 Gradignan, France.

[1]In order to avoid any possible misunderstanding, the terminology "fission product," used in the present work, corresponds to nuclei before undergoing β decay but after prompt neutron emission.

high-resolution ionization chamber and using the $\Delta E - E$ separation technique allows good nuclear charge discrimination within a mass line, yielding an accurate isotopic yield determination. Unfortunately, this experimental procedure can only be applied for fission products with a nuclear charge Z less than ~39 (Y) (i.e., in the light mass region). The use of a solid absorber located just in front of the ionization chamber increases the difference in energy loss for two successive Z values. Thus, with this technique isotopic yields have been measured up to $Z = 47$ (Ag) [19,22], but not heavier, because this energy discrimination increases with the kinetic energy of the fragment and decreases with its nuclear charge [10], making impossible the Z separation in the heavy mass region.

In order to benefit from the high performance of the Lohengrin spectrometer to study fission product characteristics also in the heavy mass region, a new experimental setup based on γ spectrometry for fission product identification has been installed at Lohengrin and is described in Sec. II. Results obtained from the ^{239}Pu(n$_{th}$,f) reaction are presented and discussed in Sec. III.

II. EXPERIMENTAL PROCEDURE

A. Sample and detection systems

The Lohengrin recoil-mass spectrometer [23] is a nuclear physics instrument that uses low-energy fission reactions for fission fragment production (Fig. 1). It allows studying fission product characteristics from thermal neutron induced fission with a very high resolution.

The target used for this experiment is a highly enriched ^{239}Pu target (99.5%) deposited on a titanium backing. Owing to the high enrichment and to the high ^{239}Pu thermal fission cross section, contributions from other fissioning nuclei are negligible. This sample (300 μg/cm^2) is placed close to the core of ILL's high-flux reactor in a thermal-neutron flux of 5.5×10^{14} n/(cm^2 s). Fission products emerging from the target are created with an ionic charge state q (ranging from about 15 to 30) and kinetic energy E_k from about 50 to 120 MeV (depending on their mass A). The selection of these fission products is performed by a combination of a magnetic (main magnet in Fig. 1) and an electric (condenser in Fig. 1) sector field, whose deflections are perpendicular to each other. At the exit slit of this parabola spectrometer, the combined action of the two fields separates ions according to their A/q and E_k/q ratios. The energy dispersion in the direction along each parabola amounts to 7.2 cm for 1% difference in kinetic energy, and the mass dispersion perpendicular to each parabola amounts to 3.24 cm for a 1% mass difference. Then a focusing magnet ("RED" magnet in Fig. 1) is installed at the exit slit of the spectrometer, which increases the particle density by a factor of 7 [24]. The flight path for the fission products is 23 m for an ~2 μs time of flight, so that fission products reach the detector before undergoing β decay.

As already mentioned, the solid absorber and high-resolution ionization chamber associated with the Lohengrin spectrometer allowed determination of mass and isotopic yields only in the light mass region [19]. In order to investigate the heavy mass region by taking advantage of the very high thermal neutron flux as well as the very high mass and energy resolutions, a new experimental setup has been developed. It is based on γ spectrometry, which is, for the first time, coupled with the spectrometer. Indeed, because β decays of fission products are often followed by γ de-excitation, these γ rays can be used to identify the fission products and to determine their yields.

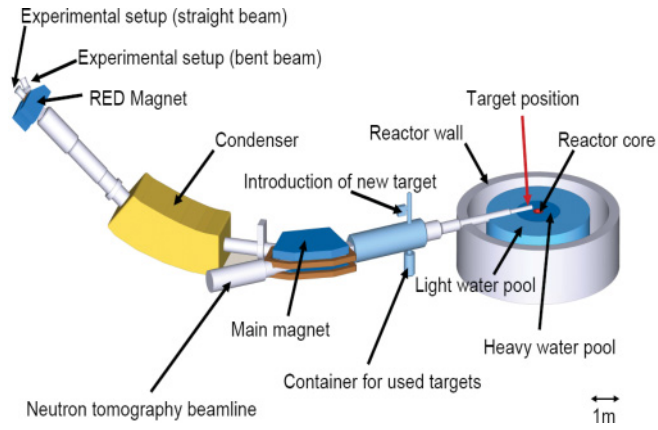

FIG. 1. (Color online) Schematic view of the Lohengrin mass spectrometer located at the Institut Laue Langevin in Grenoble, France.

For this purpose, the measurement is performed in several steps.

(i) The electric and magnetic fields of the mass spectrometer are set to select fission products with a given mass (A), ionic charge (q), and kinetic energy (E_k).
(ii) These fission products are implanted during the measuring time (typically 1 h, depending on the fission product yield) in a tape located inside a vacuum chamber that is placed at the focal point of the spectrometer.
(iii) During this measuring time, γ rays are registered with two high-efficiency germanium clover detectors HPGe placed close to the vacuum chamber (see Fig. 2).

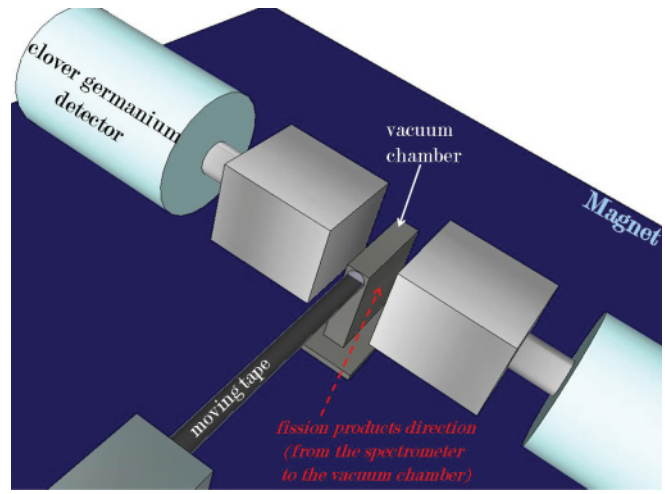

FIG. 2. (Color online) View of the experimental setup used in the present work and placed at the exit slit of the mass spectrometer.

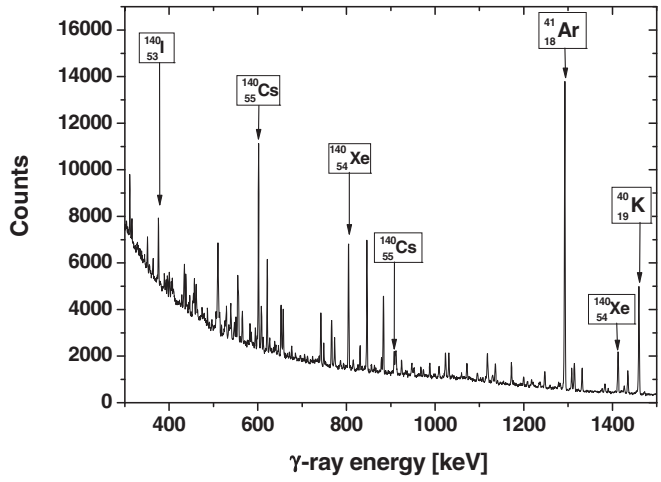

FIG. 3. Example of γ spectrum obtained after $T_{\text{meas}} = 1800$ s, for $A = 140$, $q = 22$, and $E_k = 62$ MeV. γ rays from ^{140}I, ^{140}Xe, and ^{140}Cs are clearly visible. ^{41}Ar and ^{40}K are contaminants.

(iv) Then the tape is moved to remove the residual activity, and a new measurement can start.

(v) Between two measurements, the fission product beam is blocked by an electrostatic deflector for a background determination.

In opposition to the usual experiments, which measure only a few isotopes for a given fissile nucleus, this procedure can be applied to all short-lived fission products with known γ-ray intensity ratios and decay constants. Still, certain fission products cannot be investigated because they either are stable or decay without γ-ray emission or with γ rays of an insufficiently well-known intensity. The analysis of the data is then based on the integration of Bateman equations [25] as explained in the following section.

B. Data reduction

For each measured γ spectrum, intensities of the γ rays are analyzed by using the fitting procedure TV code developed at Cologne (Germany) [26]. An example of such a γ spectrum is given in Fig. 3: it corresponds to the mass $A = 140$ (with $q = 22$ and $E_k = 22$ MeV) obtained in 0.5 h measuring time. γ rays from ^{140}I, ^{140}Xe, and ^{140}Cs can be clearly identified.

All γ rays used for the determination of the fission product yield are summarized in Table I with their branching ratios. As reported in this table, only a few γ rays (the most intense ones) were considered for a given fission product.

The analysis of a specific γ ray (after fitting the background) leads to the determination of the quantity $I_\gamma^{\text{Exp}}(A, Z, q, E_k)$, which corresponds to the measured number of γ rays emitted by a fission product with a mass number A and a nuclear charge Z, separated with an ionic charge q and a kinetic energy E_k. This quantity has to be corrected by the γ detector efficiency $\epsilon(E_\gamma)$, the γ-ray branching ratio $\text{BR}(A, Z, E_\gamma)$, and the burn-up of the ^{239}Pu target $\text{BU}(t)$ (where t corresponds to the

TABLE I. Decay γ-ray energies and their intensities used for fission product yield measurements (first isomeric states are followed by a superscript m). These nuclear data are taken from the mentioned international libraries JEFF-3.1.1 [5], NNDC [45], and LBNL [46]). An asterisk means that 10% arbitrary uncertainty was considered when nothing was mentioned in the library.

Mass	Nuclide	E_γ (keV)	BR (%)	Nuclear library
93	$_{36}$Kr	253.4	14.2 ± 2.6	JEFF-3.1.1
		323.9	24.1 ± 1.4	JEFF-3.1.1
	$_{37}$Rb	432.6	20.2 ± 2.0	JEFF-3.1.1
		986.1	7.9 ± 0.9	JEFF-3.1.1
	$_{38}$Sr	875.7	24.5 ± 1.7	JEFF-3.1.1
94	$_{37}$Rb	836.9	87 ± 3.0	NNDC
		1309.1	14.2 ± 8.0	NNDC
	$_{38}$Sr	1427.7	94 ± 0.7	JEFF-3.1.1
	$_{39}$Y	918.7	56 ± 3.0	JEFF-3.1.1
		1138.9	6 ± 0.5	JEFF-3.1.1
95	$_{37}$Rb	352	59 ± 2.0	JEFF-3.1.1
		204	18.2 ± 1.1	JEFF-3.1.1
	$_{38}$Sr	685.6	22.6 ± 1.2	JEFF-3.1.1
		2717.3	4.6 ± 0.6	JEFF-3.1.1
	$_{39}$Y	954	15.8 ± 0.7	JEFF-3.1.1
		2175.6	7 ± 0.4	JEFF-3.1.1
96	$_{38}$Sr	809.4	71.9 ± 2.6	JEFF-3.1.1
	$_{39}$Y^m	914.8	59.7 ± 2.7	JEFF-3.1.1
		617.2	57.9 ± 2.7	JEFF-3.1.1
98	$_{38}$Sr	119.4	72.9 ± 4.4	JEFF-3.1.1
	$_{39}$Y	1590.9	14.8 ± 1.4	JEFF-3.1.1
	$_{39}$Y^m	620.5	66.1 ± 3.8	JEFF-3.1.1
		647.6	52.2 ± 2.9	JEFF-3.1.1
99	$_{38}$Sr	125.1	16.1 ± 2.4	JEFF-3.1.1
	$_{39}$Y	121.8	44 ± 3.0	JEFF-3.1.1
	$_{40}$Zr	546.1	48.3 ± 2.1	JEFF-3.1.1
	$_{41}$Nb	137.7	$90.6 + 9.06^*$	JEFF-3.1.1
	$_{41}$Nb^m	97.8	6.7 ± 0.8	JEFF-3.1.1
133	$_{51}$Sb	1096.2	43 ± 2.4	JEFF-3.1.1
	$_{52}$Te	312.1	62.4 ± 0.5	JEFF-3.1.1
	$_{52}$Te^m	863.9	15.6 ± 0.8	JEFF-3.1.1
134	$_{51}$Sb^m	1279	100 ± 5.0	LBNL
	$_{52}$Te	767.2	29.6 ± 0.6	JEFF-3.1.1
		210.5	22.4 ± 0.8	JEFF-3.1.1
	$_{53}$I	847	95.4 ± 1.9	JEFF-3.1.1
		884.1	64.9 ± 1.9	JEFF-3.1.1
	$_{53}$I^m	272.1	79.1 ± 3.0	JEFF-3.1.1
136	$_{51}$Sb	2077.9	22.4 ± 2.5	JEFF-3.1.1
		333.9	18.8 ± 2.1	JEFF-3.1.1
	$_{53}$I	1321.1	24.8 ± 1.8	JEFF-3.1.1
	$_{53}$I^m	381.4	100 ± 6.0	LBNL
137	$_{53}$I	1218	13.1 ± 0.9	JEFF-3.1.1
	$_{54}$Xe	455.5	31.2 ± 0.5	JEFF-3.1.1
138	$_{53}$I	588.8	54 ± 6.3	JEFF-3.1.1
	$_{54}$Xe	258.4	31.5 ± 1.3	JEFF-3.1.1
		434.6	20.3 ± 0.8	JEFF-3.1.1
	$_{55}$Cs	1009.8	29.8 ± 0.6	JEFF-3.1.1
	$_{55}$Cs^m	191.9	15.4 ± 1.7	JEFF-3.1.1

TABLE I. *(Continued.)*

Mass	Nuclide	E_γ (keV)	BR (%)	Nuclear library
139	$_{53}$I	571.2	8.3 ± 0.7	ENDF/B-VI.8
	$_{54}$Xe	218.6	56 ± 6.0	ENDF/B-VI.8
		296.5	21.7 ± 2.4	ENDF/B-VI.8
	$_{55}$Cs	1283.2	7.1 ± 1.5	ENDF/B-VI.8
		627.2	1.5 ± 0.3	ENDF/B-VI.8
140	$_{53}$I	376.6	$90 + 9.0^*$	LBNL
	$_{54}$Xe	805.5	$20 + 2.0^*$	LBNL
		1413.6	12.2 ± 12.0	LBNL
	$_{55}$Cs	602.3	52.5 ± 16.0	LBNL
		908.3	8.56 ± 21.0	LBNL
141	$_{55}$Cs	1194	4 ± 0.3	JEFF-3.1.1
	$_{56}$Ba	190.3	46 ± 3.3	JEFF-3.1.1
		304.2	25.4 ± 1.8	JEFF-3.1.1
142	$_{55}$Cs	359.6	27.2 ± 2.7	JEFF-3.1.1
		1326.5	12.9 ± 1.3	JEFF-3.1.1
	$_{56}$Ba	255.3	20.5 ± 0.8	JEFF-3.1.1
		1204.3	14.2 ± 0.5	JEFF-3.1.1
	$_{57}$La	641.3	47.4 ± 0.5	JEFF-3.1.1
143	$_{56}$Ba	798.8	15.6 ± 3.0	LBNL
		643.8	1.55 ± 8.0	LBNL
144	$_{56}$Ba	103.9	23.3 ± 12.0	LBNL
	$_{57}$La	397.4	94.3 ± 16.0	LBNL
145	$_{56}$Ba	96.6	$17 + 1.7^*$	LBNL
		91.9	$7 + 0.7^*$	LBNL
	$_{57}$La	118.2	3.6 ± 0.6	JEFF-3.1.1
	$_{58}$Ce	724.3	44 ± 6.0	JEFF-3.1.1
		1148	9.6 ± 1.4	JEFF-3.1.1
146	$_{56}$Ba	251.2	19.6 ± 5.0	LBNL
	$_{57}$La	924.6	7.5 ± 0.4	JEFF-3.1.1
	$_{57}$La^m	514.6	23.8 ± 19.0	LBNL
		502.9	19.7 ± 15.0	LBNL
	$_{58}$Ce	316.7	56.2 ± 3.0	JEFF-3.1.1
147	$_{57}$La	117.7	12 ± 1.0	JEFF-3.1.1
		186.3	6.5 ± 0.6	JEFF-3.1.1
	$_{58}$Ce	268.8	6.3 ± 0.4	JEFF-3.1.1
		92.9	4 ± 0.4	JEFF-3.1.1
148	$_{57}$La	158.5	55.6 ± 1.4	JEFF-3.1.1
		989.9	9.3 ± 0.3	JEFF-3.1.1
	$_{58}$Ce	269.5	17 ± 9.0	JEFF-3.1.1
151	$_{59}$Pr	484.5	9.3 ± 5.0	LBNL
		495.3	8.5 ± 6.0	LBNL
	$_{60}$Nd	116.8	39 ± 5.0	LBNL
		255.7	14.8 ± 3.0	LBNL
152	$_{59}$Pr	226.7	7.8 ± 7.8	LBNL
	$_{60}$Nd	278.6	29 ± 17.0	LBNL

elapsed time from the beginning of the ^{239}Pu sample irradiation):

$$I_\gamma^{\mathrm{cor}} = \frac{I_\gamma^{\mathrm{Exp}}(A, Z, q, E_k)}{\epsilon(E_\gamma) \times \mathrm{BR}(A, Z, E_\gamma) \times \mathrm{BU}(t)}. \quad (1)$$

These three corrections (germanium efficiency, branching ratio, and burn-up) were determined as follows.

TABLE II. γ-ray energies (E_γ) and their branching ratio (BR) from ^{96m}Y decay (data taken from JEFF-3.1.1 [5]). These γ rays were used for determination of the detection efficiency.

E_γ (keV)	BR (%)
146.7	36.4 ± 2.6
173.7	2.4 ± 0.4
363.1	28.5 ± 5.1
475.6	3.1 ± 0.1
617.2	57.9 ± 2.6
631.5	10.5 ± 1.7
643.7	1.5 ± 0.1
690.0	1.6 ± 0.1
804.7	1.6 ± 0.1
906.2	27.6 ± 4.4
914.8	59.7 ± 2.6
960.2	3.5 ± 0.3
979.2	3.6 ± 0.3
1006.4	1.1 ± 0.1
1107.2	47.0 ± 1.0
1114.6	1.8 ± 0.1
1185.0	$3.4 \pm 0.$
1222.9	33.4 ± 3.5
1279.4	0.9 ± 0.1
1592.9	1.5 ± 0.2
1750.6	87.8 ± 0.8
1897.6	5.1 ± 0.1
2226.2	5.5 ± 0.3

1. Germanium efficiency

In order to determine the relative germanium detector efficiency, a fission product beam of mass 96 from the spectrometer was implanted on the tape, allowing the detection of a large number of γ rays stemming from the decay of ^{96}Sr and ^{96m}Y with energies ranging from 150 keV to 2.2 MeV (see Table II). The γ-ray energy area of this extended calibration source is rather identical to the one covered by the fission products that will be measured. Germanium detectors are placed far enough from the vacuum chamber, so that the sum peak effect can be neglected. In principle, the germanium efficiency curve can be well described by fitting experimental data with the following equation [27]:

$$\epsilon(E_\gamma) = \frac{\mathcal{K}[\tau + \sigma\,\mathcal{Q}\exp(-\mathcal{R}E_\gamma)]}{\tau + \sigma}[1 - \exp(-\mathcal{P}(\tau + \sigma)]. \quad (2)$$

In Eq. (2), τ and σ stand, respectively, for the photoelectric absorption coefficient and the Compton absorption coefficient at E_γ energy. $\mathcal{K}$, $\mathcal{Q}$, $\mathcal{R}$, and $\mathcal{P}$ are four free parameters. However, owing to the limited γ-energy range of the investigated fission products (from about 100 keV up to about 2.7 MeV), such a complete formula is not needed and experimental data (weighted by their error bars) were fitted using the following simplified equation:

$$\ln(\epsilon) = \sum_{i=1}^{N} a_i [\ln(E_\gamma)]^{i-1}, \quad (3)$$

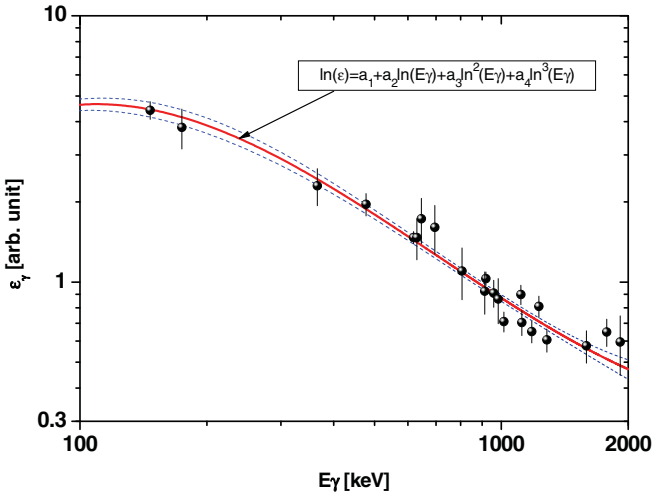

FIG. 4. (Color online) Germanium detector efficiency as a function of γ-ray energy. The measurement was carried out using a mass-96 beam. Experimental points were fitted using Eq. (3).

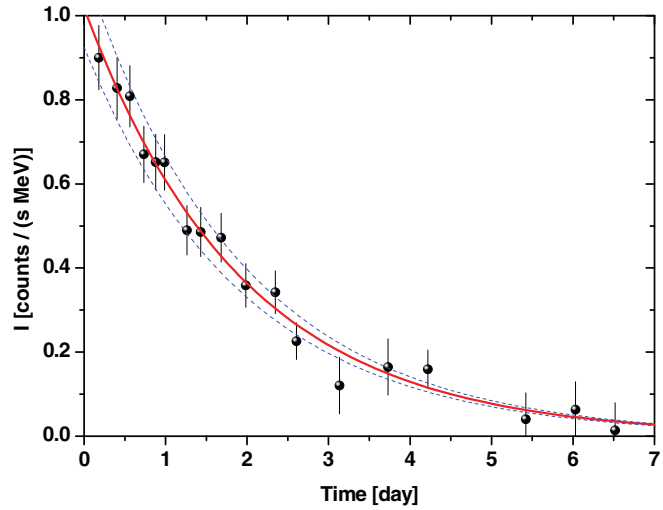

FIG. 5. (Color online) Example of burn-up measurement obtained for one ^{239}Pu target used during the experiment. I is the measured intensity of the 334-keV γ ray from the ^{136}Te decay. The fit on the experimental points [solid (red) curve)] was performed using Eq. (4).

where a_i are free parameters. As shown in Fig. 4, Eq. (3) with $N = 4$ was used to perform the fit.

2. Nuclear decay data

As shown in Eq. (1), each γ peak must be normalized to its branching ratio. The half-lives and branching ratio values used in the present work come from various nuclear data libraries (see Table I) and were chosen according to the consistency of the data and their associated uncertainties.

3. ^{239}Pu target burn-up

Finally, the ^{239}Pu target burn-up has to be taken into account [28]. This burn-up was determined by measuring periodically (roughly every 12 h) the intensity of the 334-keV γ ray from the ^{136}Te decay. An example of the measured burn-up is given in Fig. 5. The experimental points are well described by using two decreasing exponential functions, one for describing the "slow" target burn-up owing to nuclear transmutation and self-sputtering and another, "fast" one for describing all phenomena that occur during the first hours of the target combustion (nuclear heating of the target to its equilibrium temperature):

$$\mathrm{BU}(t) = I_0 \exp(-\lambda_0 t) + I_1 \exp(-\lambda_1 t), \tag{4}$$

where I_0, I_1, λ_0, and λ_1 are four free parameters deduced from the fit.

The quantity defined in Eq. (1) is correlated with the number of fission products that are formed at time t (after the beginning of the implantation on the tape), by the following equation:

$$I_\gamma^{\mathrm{cor}}(A, Z, q, E_k) = k \int_0^{T\mathrm{meas}} \lambda(A, Z) \times N(A, Z, q, E_k, t)dt, \tag{5}$$

where T_{meas} is the measuring time and k a normalization constant that is discussed in Sec. II C2. The number of fission products arriving from the target to the tape is related to the partial independent yield through Bateman's equation:

$$\begin{aligned}\frac{dN(A, Z, q, E_k, t)}{dt} &= Y(A, Z, q, E_k)\mathcal{F} - \lambda(A, Z)N(A, Z, q, E_k, t) \\ &\quad + \sum_{j\geqslant 1} \lambda(A, Z-j)N(A, Z-j, q, E_k, t).\end{aligned} \tag{6}$$

The first term in Eq. (6) corresponds to the production of the $N(A, Z, q, E_k, t)$ nuclei by fission: $Y(A, Z, q, E_k)$ is the independent fission yield and $\mathcal{F}$ stands for the fission rate, which is included in the normalization constant k appearing in Eq. (5). The second term accounts for the disappearance of the (A, Z, q, E_k) nuclei by β^- decay. Finally, the third term corresponds to the creation of the (A, Z, q, E_k) nuclei by successive β^- decays of the $(A, Z-j, q, E_k)$ nuclei, which are also directly produced by fission. In the case of the isomeric state, all available decays are taken into account.

The differential equation from Eq. (6) was resolved by the fourth-order Runge-Kutta method, and in parallel, the partial independent fission product yields $Y(A, Z, q, E_k)$ have been determined from both Eq. (5) and Eq. (6) with a bisection method.

For fission products, where more than one γ ray can be determined quantitatively, the partial independent fission product yield is calculated from the weighted average of all considered γ rays.

C. Independant isotopic yield determination

1. Integration over kinetic energies and ionic charges

The procedure described in the previous section allows the determination of the partial independent yield $Y(A, Z, q, E_k)$. In principle, in order to calculate the independent yield

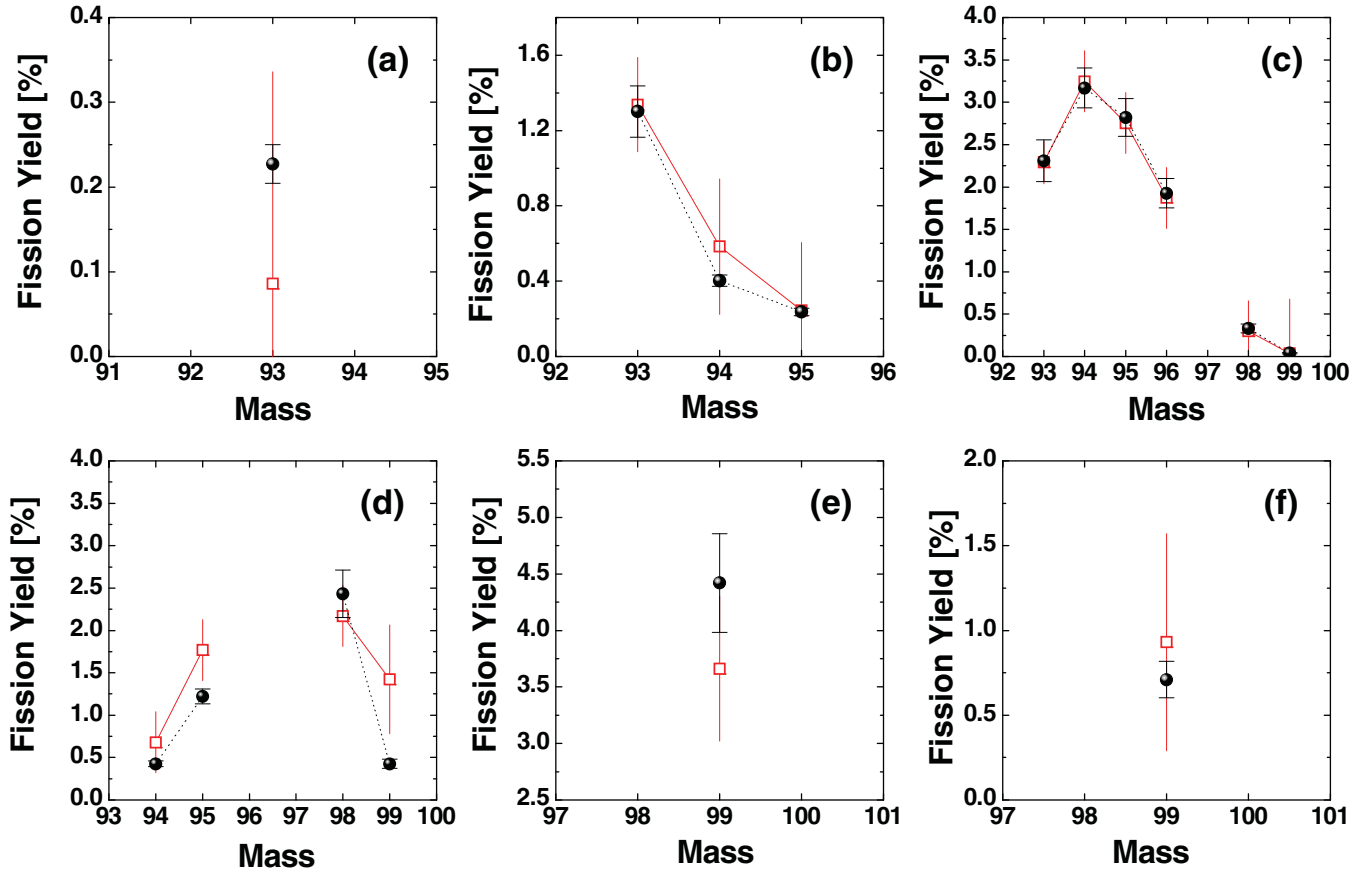

FIG. 6. (Color online) Isotopic yield measured in the light mass region by γ-ray spectroscopy [present work; filled (black) circles], compared with Schmitt's data [16] [open (red) squares], obtained with an ionization chamber: $_{36}$Kr (a), $_{37}$Rb (b), $_{38}$Sr (c), $_{39}$Y (d), $_{40}$Zr (e), and $_{41}$Nb (f).

$Y(A, Z)$, a complete scan over all kinetic energies and all ionic charge states is needed:

$$Y(A, Z) = \int \sum_{q} Y(A, Z, q, E_k) dE_k. \tag{7}$$

However, this method would be too time-consuming. Therefore, regardless of the fission region, each $Y(A, Z)$ can be determined by only measuring various kinetic energies at the average ionic charge $\overline{q}$ and by measuring various ionic charge states at the average kinetic energy $\overline{E_k}$:

$$Y(A, Z) = \frac{\int Y(A, Z, \overline{q}, E_k) dE_k \times \sum_q Y(A, Z, q, \overline{E_k})}{Y(A, Z, \overline{q}, \overline{E_k})}. \tag{8}$$

Measured ionic charge state and kinetic energy distributions are adjusted with Gaussian functions, and both $\int Y(A, Z, \overline{q}, E_k) dE_k$ and $\sum_q Y(A, Z, q, \overline{E_k})$ quantities are determined from the values of the Gaussian integrals. The shapes of these distributions are similar for all masses if one considers the isotopes without a nanosecond isomeric state (see Sec. III B4). If no correlation exists between the ionic charge state and the kinetic energy, the Eq. (8) is equivalent to the exact Eq. (7). Nevertheless, in the considered kinetic energy and ionic-charge-state ranges, a light correlation has been observed. It leads to an additional uncertainty, which is discussed in Sec. III.

2. *Normalization*

Because only the relative germanium detector efficiency is known, the absolute independent yield cannot be determined, and therefore, our data need to be normalized [parameter k in Eq. (5)]. To do this, the sum of the measured isotopic yields has been equalized to the sum of isotopic yields available in the JEFF-3.1.1 library for the same fission products. This sum (over the 65 measured fission products) represents 90.67% of the total fission yields (200%).

D. Validation of the experimental setup

In order to test the correct functioning of our new experimental setup, various fission product yields from ^{239}Pu(n$_{th}$,f) were measured in the light mass region and compared with the ones obtained previously by Schmitt *et al.* [16]. This measurement was performed in 1984 at the Lohengrin mass spectrometer, but with a completely different experimental setup (ionization chamber). Within the error bars, a good agreement can be achieved as shown in Fig. 6, except for the yttrium element, for which differences between both experiments are a bit larger.

TABLE III. ^{239}Pu(n_{th}, f) fission product yields measured in the light mass region by γ-ray spectroscopy (present work). Statistical (stat.) and systematic (syst.) uncertainties as well as uncertainties owing to nuclear data are listed (in %). The total uncertainty [Eq. (9)] is given in the last column. First isomeric states are indicated by a superscript m.

Mass	Nuclide	Yield (%)	Uncertainty					
			Stat. (%)	Syst. (%)	$\epsilon(E_\gamma)$	Nuclear data (%)	Decay (%)	Total (%)
93	$_{36}$Kr	0.227	1.17	3.40	3.78	5.54	0.00	10.01
	$_{37}$Rb	1.301	1.08	3.40	2.79	7.47	0.34	10.43
	$_{38}$Sr	2.31	1.08	3.40	3.64	6.94	0.05	10.68
94	$_{37}$Rb	0.402	1.08	3.40	2.34	3.44	0.00	7.64
	$_{38}$Sr	3.168	1.08	3.40	2.89	0.74	0.03	7.41
	$_{39}$Y	0.426	1.08	3.40	2.40	4.51	0.35	8.23
95	$_{37}$Rb	0.236	1.08	3.40	3.82	2.96	0.00	8.81
	$_{38}$Sr	2.82	1.08	3.40	1.70	4.92	0.01	7.90
	$_{39}$Y	1.221	1.08	3.40	1.88	3.50	0.28	7.27
96	$_{38}$Sr	1.927	1.08	3.40	3.76	3.62	0.00	9.00
	$_{39}$Y^m	1.678	1.08	3.40	2.72	3.25	0.50	7.91
	$_{39}$Y	1.956	1.08	3.40	2.72	9.46	2.89	12.23
	$_{39}$Y^m	0.477	1.08	3.40	2.93	3.99	1.77	8.60
98	$_{38}$Sr	0.331	4.04	3.40	6.67	6.04	0.00	15.35
	$_{39}$Y	1.956	1.08	3.40	2.72	9.46	2.89	12.23
	$_{39}$Y^m	0.477	1.08	3.40	2.93	3.99	1.77	8.60
99	$_{38}$Sr	0.04	1.08	3.40	6.60	14.91	0.00	18.57
	$_{39}$Y	0.426	1.08	3.40	6.64	6.82	0.35	13.05
	$_{40}$Zr	4.419	1.08	3.40	4.37	4.35	0.89	9.90
	$_{41}$Nb	0.568	1.08	3.40	6.45	10.00	0.58	14.83
	$_{41}$Nb^m	0.142	1.08	3.40	6.96	11.94	0.18	16.54

This agreement was very important to validate both the good functioning of our experimental setup and the procedure used for the data analysis. It gives confidence for extending this method to the heavy mass region.

III. RESULTS AND DISCUSSION

A. Accuracy of data

Potential sources of uncertainties induced by our experimental set-up as well as by the procedure used for the data analysis were identified and are discussed in this section. This discussion is very similar to the one presented by Laurec *et al*. [29].

1. Statistical uncertainties: Δ_{stat}

(i) The analysis of the measured γ spectra was performed using the TV code [26]. In particular, this code allows the performance of a fit of a selected γ peak and to deduce its area after fitting the background. The code deals by itself with statistical uncertainties as well as errors owing to the fit.

(ii) An additional statistical effect is caused by the thermal neutron flux stability. To take these fluctuations into account, we first consider the global reactor heat, which is recorded as a function of time. It is directly proportional to global neutron flux variations and gives a rough idea about neutron flux variations but does not reproduce local fluctuations exactly. This is why subsequently variations have been more accurately followed by measuring a given mass frequently during the experiment. Based on measurement reproducibility, variations have been estimated to be lower than 0.6%.

Both statistical uncertainties were combined quadratically to get the total statistical uncertainty (Δ_{stat}).

2. Systematic uncertainties: Δ_{syst}

(i) ^{239}*Pu target burn-up*. The uncertainty owing to the burn-up of the sample is deduced from the weighted fit performed on the burn-up measurement (see Fig. 5).

(ii) *Mass yield determination procedure*. As explained in Sec. II C1, the isotopic yield is determined by measuring the kinetic energy distribution associated with the mean ionic charge state $\bar{q}$ and the ionic-charge-state distribution associated with the mean kinetic energy $\bar{E}_k$ [Eq. (8)]. As already stated, this procedure is rigorous only when q and E_k are uncorrelated, which is not strictly the case [30,31]. In order to quantify properly the uncertainty owing to this correlation, one light mass ($A = 98$) and one heavy mass ($A = 136$) have been studied for all ionic-charge-state and kinetic energy combinations. Thus, yields have been determined directly by summing all these combinations without any approximation [Eq. (7)]. It has shown that the approximation owing to the use of Eq. (8) leads to an additional uncertainty of less than 1.3% [31].

TABLE IV. Same as Table III but for fission products belonging to the heavy mass region.

Mass	Nuclide	Yield (%)	Uncertainty					
			Stat. (%)	Syst. (%)	$\epsilon(E_\gamma)$	Nucl. data (%)	Decay (%)	Total (%)
133	$_{51}$Sb	1.231	1.62	3.40	3.30	5.53	0.00	9.99
	$_{52}$Te	1.881	1.08	3.40	5.22	0.80	1.04	9.79
	$_{52}$Te^m	2.898	1.25	3.40	3.66	5.13	0.32	9.78
134	$_{51}$Sb^m	0.571	1.25	3.40	3.06	5.00	0.00	9.19
	$_{52}$Te	3.581	1.71	3.40	3.21	1.76	0.01	8.50
	$_{53}$I	1.496	1.00	3.40	2.59	1.65	9.92	12.24
	$_{53}$I^m	1.116	1.80	3.40	5.43	3.79	36.90	38.59
136	$_{52}$Te	0.527	3.65	3.40	2.10	7.90	0.00	12.08
	$_{53}$I	0.807	1.08	3.40	3.01	7.26	1.13	10.49
	$_{53}$I^m	2.483	1.71	3.40	4.92	6.00	0.74	11.71
137	$_{53}$I	2.244	1.52	3.40	3.13	6.87	0.00	10.59
	$_{54}$Xe	3.653	1.90	3.40	4.65	1.60	0.48	10.08
138	$_{53}$I	0.475	1.80	3.40	4.25	11.65	0.00	15.00
	$_{54}$Xe	4.687	1.17	3.40	3.58	2.85	0.01	8.63
	$_{55}$Cs	0.564	2.67	3.40	3.42	2.01	6.03	11.42
	$_{55}$Cs^m	0.857	2.67	3.40	5.95	11.04	33.42	37.19
139	$_{53}$I	0.133	1.08	3.40	4.30	8.43	0.00	12.18
	$_{54}$Xe	3.115	2.18	3.40	3.90	7.70	0.03	12.21
	$_{55}$Cs	2.263	3.65	3.40	2.46	14.52	0.59	17.37
140	$_{53}$I	0.068	1.80	3.40	4.93	10.00	0.00	14.24
	$_{54}$Xe	1.512	1.52	3.40	2.30	7.07	0.05	10.11
	$_{55}$Cs	2.932	1.71	3.40	2.73	1.91	0.79	8.11
141	$_{55}$Cs	3.135	1.52	3.40	3.16	7.50	0.00	11.03
	$_{56}$Ba	1.583	1.43	3.40	3.95	5.04	0.27	10.13
142	$_{55}$Cs	0.953	1.00	3.40	2.57	7.07	0.00	9.93
	$_{56}$Ba	3.582	1.52	3.40	2.74	2.61	0.01	8.09
	$_{57}$La	0.406	1.43	3.40	4.12	1.05	4.88	10.25
143	$_{56}$Ba	2.851	1.52	3.40	3.78	1.92	0.00	8.92
	$_{57}$La	1.045	1.52	3.40	4.12	5.16	0.12	10.41
144	$_{56}$Ba	2.679	1.99	3.40	6.87	0.52	0.00	12.28
	$_{57}$La	1.228	1.99	3.40	4.85	1.70	1.81	10.54
145	$_{56}$Ba	0.824	1.99	3.40	4.96	7.07	0.00	12.54
	$_{57}$La	1.796	1.52	3.40	6.68	16.67	0.77	20.32
	$_{58}$Ce	0.430	1.80	3.40	2.49	9.96	2.76	12.89
146	$_{56}$Ba	0.511	1.90	3.40	5.55	2.55	0.00	11.14
	$_{57}$La	0.293	1.08	3.40	3.56	5.33	1.00	9.70
	$_{57}$La^m	0.742	1.34	3.40	3.17	5.51	1.71	9.79
	$_{58}$Ce	0.793	2.38	3.40	5.20	5.34	0.02	12.20
147	$_{57}$La	0.655	1.71	3.40	4.47	6.19	0.00	11.40
	$_{58}$Ce	1.619	1.90	3.40	4.31	5.36	0.25	11.00
148	$_{57}$La	0.191	1.80	3.40	3.02	1.98	0.00	8.46
	$_{58}$Ce	0.920	2.38	3.40	5.44	5.29	0.07	12.41
151	$_{59}$Pr	0.419	1.34	3.40	3.21	4.28	0.00	9.03
	$_{60}$Nd	0.289	1.90	3.40	4.26	1.25	0.14	9.64
152	$_{59}$Pr	0.028	2.28	3.40	5.70	5.13	0.00	12.49
	$_{60}$Nd	0.534	2.18	3.40	5.39	5.86	0.00	12.44

(iii) *Normalization factor*. Uncertainties owing to our normalization procedure. (see Sec. II C2) have been estimated at 1.5%.

The total systematic uncertainty (Δ_{syst}) is calculated by summing these three contributions.

TABLE V. Sum of the ground-state and the first isomeric-state yields ($S = Y^{GS} + Y^m$) and ratio between the isomeric yield and the sum [$R = Y^m/(Y^{GS} + Y^m)$]. Results obtained in this work (Loh.) are compared with those from JEFF-3.1.1 [5].

Mass	Nuclide	$S_{Loh.}$ (%)	$S_{JEFF\text{-}3.1.1}$ (%)	$R_{Loh.}$ (%)	$R_{JEFF\text{-}3.1.1}$ (%)
98	$_{39}$Y	2.433 ± 0.280	2.310 ± 0.512	19.6 ± 3.3	80.8 ± 25.3
99	$_{41}$Nb	0.710 ± 0.108	0.850 ± 0.280	20.0 ± 4.2	18.8 ± 8.7
133	$_{52}$Te	4.779 ± 0.468	4.646 ± 0.534	60.6 ± 8.4	70.7 ± 11.5
134	$_{53}$I	2.612 ± 0.614	2.248 ± 0.545	42.7 ± 11.3	42.4 ± 14.6
136	$_{53}$I	3.290 ± 0.375	3.358 ± 0.591	75.5 ± 11.7	70.1 ± 17.4
138	$_{55}$Cs	1.420 ± 0.383	1.033 ± 0.348	60.3 ± 17.7	58.7 ± 28.0
146	$_{57}$La	1.035 ± 0.101	1.258 ± 0.213	71.7 ± 9.9	64.3 ± 15.4

3. *Uncertainties owing to the detection efficiency:* $\Delta_{\epsilon(E_\gamma)}$

As for the target burn-up uncertainty, the uncertainty owing to the detection efficiency is determined from the weighted fit performed on the experimental data (see Fig. 4).

4. *Uncertainties owing to the nuclear data:* Δ_{ND}

Uncertainties related to nuclear data (mainly γ-ray branching ratios) have an important impact on the final isotopic yield uncertainties. These uncertainties, denoted Δ_{ND}, were taken from nuclear data libraries mentioned in Table I.

5. *Uncertainties owing to the mother's data:* Δ_{Decay}

Owing to the β-decay constants that appear in the Bateman equation [Eq. (6)], the uncertainty of the mother nucleus yield has to be propagated to the uncertainty of the daughter nucleus yield. This uncertainty is evaluated by summing the Δ_{syst}, $\Delta_{\epsilon(E_\gamma)}$, and Δ_{ND} quantities of the mother nuclei, but weighted by the ratio between the detected mother nuclei and the detected daughter nuclei. Uncertainties are propagated from the first measured nuclei, unmeasured isotopes not being taken into account.

6. *Total uncertainties*

The total uncertainty is then calculated as follows:

$$\Delta_{tot} = \sqrt{(\Delta_{stat} + \Delta_{syst} + \Delta_{\epsilon(E_\gamma)})^2 + \Delta_{ND}^2 + \Delta_{Decay}^2}. \quad (9)$$

B. Isotopic yields

Isotopic yield values for the 65 measured fission products (19 in the light mass region and 46 in the heavy mass region)

TABLE VI. ^{239}Pu(n_{th}, f) fission product yields (in %) measured in the light mass region (present work) and compared with the three main libraries: JEFF-3.1.1 [5], ENDF/B-VII.0 [6] and JENDL-4.0 [7]. Relative differences (relat. diff.) are given for each library. Isomeric states are indicated by a superscript m.

Mass	Nuclide	Present work	JEFF-3.1.1	Relat. diff. (%)	ENDF/-B-VII.0	Relat. diff. (%)	JENDL-4.0	Relat. diff. (%)
93	$_{36}$Kr	0.227 ± 0.023	0.109 ± 0.037	-108.257	0.067 ± 0.005	-238.806	0.064 ± 0.005	-254.688
	$_{37}$Rb	1.301 ± 0.136	1.57 ± 0.313	17.134	1.355 ± 0.081	3.985	1.355 ± 0.081	3.985
	$_{38}$Sr	2.31 ± 0.247	1.988 ± 0.333	-16.197	2.144 ± 0.129	-7.743	2.144 ± 0.129	-7.743
94	$_{37}$Rb	0.402 ± 0.031	0.677 ± 0.202	40.620	0.704 ± 0.113	42.898	0.704 ± 0.113	42.898
	$_{38}$Sr	3.168 ± 0.235	3.061 ± 0.327	-3.496	2.925 ± 0.175	-8.308	2.925 ± 0.175	-8.308
	$_{39}$Y	0.426 ± 0.035	0.591 ± 0.205	27.919	0.675 ± 0.108	36.889	0.675 ± 0.108	36.889
95	$_{37}$Rb	0.236 ± 0.021	0.258 ± 0.087	8.527	0.432 ± 0.099	45.370	0.432 ± 0.099	45.370
	$_{38}$Sr	2.82 ± 0.223	2.987 ± 0.432	5.591	2.612 ± 1.175	-7.963	2.612 ± 1.175	-7.963
	$_{39}$Y	1.221 ± 0.089	1.586 ± 0.413	23.014	1.678 ± 0.755	27.235	1.678 ± 0.755	27.235
96	$_{38}$Sr	1.927 ± 0.174	2.011 ± 0.403	4.177	1.822 ± 0.82	-5.763	1.822 ± 0.82	-5.763
	$_{39}$Y^m	1.678 ± 0.133	1.473 ± 0.281	-13.917	2.238 ± 1.007	25.022	2.235 ± 1.006	24.922
98	$_{38}$Sr	0.331 ± 0.051	0.231 ± 0.081	-43.290	0.327 ± 0.209	-1.223	0.327 ± 0.209	-1.223
	$_{39}$Y	1.956 ± 0.239	0.444 ± 0.098	-340.541	1.187 ± 0.38	-64.785	0.361 ± 0.115	-441.828
	$_{39}$Y^m	0.477 ± 0.041	1.866 ± 0.413	74.437	1.187 ± 0.38	59.815	2.013 ± 0.644	76.304
99	$_{38}$Sr	0.04 ± 0.007	0.038 ± 0.013	-5.263	0.037 ± 0.024	-8.108	0.037 ± 0.024	-8.108
	$_{39}$Y	0.426 ± 0.056	1.294 ± 0.356	67.079	1.444 ± 0.159	70.499	1.444 ± 0.159	70.499
	$_{40}$Zr	4.419 ± 0.438	4.005 ± 0.488	-10.337	3.763 ± 1.204	-17.433	3.763 ± 1.204	-17.433
	$_{41}$Nb	0.568 ± 0.084	0.691 ± 0.227	17.800	0.075 ± 0.012	-657.333	0.776 ± 0.124	26.804
	$_{41}$Nb^m	0.142 ± 0.023	0.16 ± 0.053	11.250	0.881 ± 0.564	83.882	0.18 ± 0.115	21.111

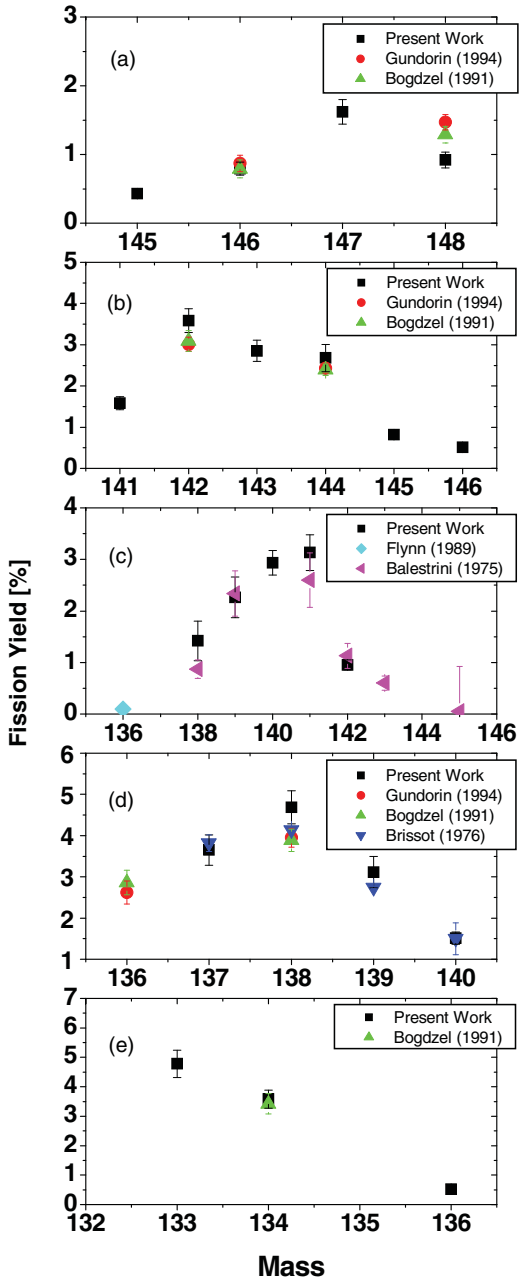

FIG. 7. (Color online) Isotopic yields obtained in this work in the heavy mass region and compared with data from the literature: $_{58}$Ce (a), $_{56}$Ba (b), $_{55}$Cs (c), $_{54}$Xe (d), and $_{52}$Te (e).

with their uncertainties are given in Table III (light fission products) and Table IV (heavy fission products).

1. Comparison with data from the literature

Our measurements performed in the heavy mass region were compared with the following data coming from the EXFOR database (see Fig. 7):

(i) Gundorin *et al.* [32]: $^{136}_{54}$Xe, $^{138}_{54}$Xe, $^{142}_{56}$Ba, $^{144}_{56}$Ba, $^{146}_{58}$Ce, $^{148}_{58}$Ce.

(ii) Bogdzel *et al.* [33]: $^{134}_{52}$Te, $^{136}_{54}$Xe, $^{138}_{54}$Xe, $^{142}_{56}$Ba, $^{144}_{56}$Ba, $^{146}_{58}$Ce, $^{148}_{58}$Ce.

(iii) Brissot *et al.* [34]: $^{137}_{54}$Xe, $^{138}_{54}$Xe, $^{139}_{54}$Xe, $^{140}_{54}$Xe.

(iv) Balestrini *et al.* [35]: $^{138}_{55}$Cs, $^{139}_{55}$Cs, $^{141}_{55}$Cs, $^{142}_{55}$Cs, $^{143}_{55}$Cs, $^{145}_{55}$Cs.

(v) Flynn *et al.* [36]: $^{136}_{55}$Cs.

As shown in Fig. 7, a general good agreement among all measured nuclear charges was found, except for $^{138}_{55}$Cs and $^{148}_{58}$Ce fission yields. Note that for both masses, 138 and 148, we have observed a strong deformed ionic-charge-state distribution, which corresponds to the presence of a nanosecond isomeric state (see Sec. III B4). However, it is probably not enough to explain the observed differences between the literature values and our data.

2. Comparison with evaluated nuclear data files

Our data are compared with the three main libraries (JEFF-3.1.1 [5], ENDB/B-VII.0 [6], and JENDL-4.0 [7]) in Table VI (light fission products) and Table VII (heavy fission products). The relative differences (derived as $1 - M/E$, where M corresponds to our measured data, and E to the evaluated yield) are also reported in these tables. In addition, the yields obtained in this work are plotted in Fig. 8 with the JEFF-3.1.1 yields.

One of the most important points that can be mentioned is the reduction of uncertainties for a large number of nuclei. This is illustrated in Fig. 9, where histograms of the 65 fission product yield uncertainties are given for both our data (top) and the JEFF-3.1.1 data (bottom). The average yield uncertainty reaches 11.9% (our measurements) and 23.3% (JEFF-3.1.1), respectively, which corresponds to a reduction of a factor of nearly 2. Nevertheless, some of them still show important uncertainties, which is partly caused by our poor knowledge of the decay data available in nuclear libraries and/or because of the difficulty of measuring low-intensity γ rays.

For the large majority of fission products, a very good agreement between the Lohengrin data and the JEFF-3.1.1 values is achieved. However, nine fission products (over the 65 measured nuclei) are not within the error bars (at 1σ): ^{98}Y, ^{99}Y, ^{133}Te, ^{134}Sb, ^{142}Ce, ^{146}Ba, ^{147}Ce, ^{152}Pr, and ^{152}Nd. In each case, our measurements are not in agreement with any of the three data libraries, except for the ^{133}Te yield, which is in accordance with ENDF/B-VII.0.

3. Isomeric-to-ground-state ratio

Yields of both ground state and isomeric state were measured for the following seven fission products: $^{98}_{39}$Y, $^{99}_{41}$Nb, $^{133}_{52}$Te, $^{134}_{53}$I, $^{136}_{53}$I, $^{138}_{55}$Cs, and $^{146}_{57}$La. For each fission product, the sum of the ground-state yield (Y^{GS}) and the isomeric-state yield (Y^m) is reported ($S = Y^{\mathrm{GS}} + Y^m$). The ratio of the isomeric-state yield to the sum ($R = Y^m/(Y^{\mathrm{GS}} + Y^m)$ is also listed in Table V.

The R and S quantities are compared with the JEFF-3.1.1 values. From Table V, various comments can be made.

TABLE VII. Same as Table VI but for fission products belonging to the heavy mass region.

Mass	Nuclide	Present work	JEFF−3.1.1	Relat. diff. (%)	ENDF B−VII.0	Relat. diff. (%)	JENDL−4.0	Relat. diff. (%)
133	$_{51}$Sb	1.231 ± 0.123	1.265 ± 0.368	2.688	1.174 ± 0.094	−4.855	1.173 ± 0.094	−4.945
	$_{52}$Te	1.881 ± 0.183	1.361 ± 0.156	−38.207	1.766 ± 0.194	−6.512	1.364 ± 0.150	−37.903
	$_{52}$Te^{m}	2.898 ± 0.284	3.285 ± 0.377	11.781	2.891 ± 0.173	−0.242	3.292 ± 0.198	11.968
134	$_{51}$Sb^{m}	0.571 ± 0.052	0.195 ± 0.068	−192.821	0.199 ± 0.128	−186.935	0.280 ± 0.179	−103.929
	$_{52}$Te	3.581 ± 0.304	4.110 ± 0.581	12.871	4.397 ± 0.264	18.558	4.397 ± 0.264	18.558
	$_{53}$I	1.496 ± 0.183e	1.294 ± 0.314	−15.611	1.436 ± 0.086	−4.178	1.509 ± 0.091	0.861
	$_{53}$I^{m}	1.116 ± 0.431	0.954 ± 0.231	−16.981	1.184 ± 0.379	5.743	1.111 ± 0.355	−0.450
136	$_{52}$Te	0.527 ± 0.064	0.68 ± 0.216	22.500	0.506 ± 0.324	−4.150	0.506 ± 0.324	−4.150
	$_{53}$I	0.807 ± 0.085	1.005 ± 0.177	19.701	1.250 ± 0.400	35.440	0.864 ± 0.277	6.597
	$_{53}$I^{m}	2.483 ± 0.291	2.353 ± 0.414	−5.525	1.642 ± 0.131	−51.218	2.027 ± 0.162	−22.496
137	$_{53}$I	2.244 ± 0.238	2.177 ± 0.519	−3.078	2.299 ± 0.138	2.392	2.299 ± 0.138	2.392
	$_{54}$Xe	3.653 ± 0.368	3.949 ± 0.564	7.496	3.684 ± 0.147	0.841	3.683 ± 0.147	0.815
138	$_{53}$I	0.475 ± 0.071	0.663 ± 0.223	28.356	1.272 ± 0.102	62.657	1.272 ± 0.102	62.657
	$_{54}$Xe	4.687 ± 0.405	4.364 ± 0.463	−7.401	3.926 ± 0.110	−19.384	3.925 ± 0.110	−19.414
	$_{55}$Cs	0.564 ± 0.064	0.427 ± 0.144	−32.084	0.308 ± 0.049	−83.117	0.372 ± 0.060	−51.613
	$_{55}$Cs^{m}	0.857 ± 0.319	0.606 ± 0.204	−41.419	0.593 ± 0.379	−44.519	0.529 ± 0.338	−62.004
139	$_{53}$I	0.133 ± 0.016	0.198 ± 0.069	32.828	0.319 ± 0.073	58.307	0.319 ± 0.073	58.307
	$_{54}$Xe	3.115 ± 0.380	3.231 ± 0.518	3.590	2.792 ± 0.112	−11.569	2.792 ± 0.112	−11.569
	$_{55}$Cs	2.263 ± 0.393	2.303 ± 0.512	1.737	2.324 ± 0.535	2.625	2.324 ± 0.534	2.625
140	$_{53}$I	0.068 ± 0.010	0.028 ± 0.010	−142.857	0.059 ± 0.038	−15.254	0.059 ± 0.038	−15.254
	$_{54}$Xe	1.512 ± 0.153	1.648 ± 0.387	8.252	1.540 ± 0.043	1.818	1.540 ± 0.043	1.818
	$_{55}$Cs	2.932 ± 0.238	2.772 ± 0.464	−5.772	2.277 ± 0.364	−28.766	2.276 ± 0.364	−28.822
141	$_{55}$Cs	3.135 ± 0.346	2.915 ± 0.450	−7.547	2.867 ± 0.459	−9.348	2.867 ± 0.459	−9.348
	$_{56}$Ba	1.583 ± 0.160	1.743 ± 0.428	9.180	1.828 ± 0.420	13.403	1.828 ± 0.420	13.403
142	$_{55}$Cs	0.953 ± 0.095	1.524 ± 0.367	37.467	1.397 ± 0.321	31.782	1.396 ± 0.321	31.734
	$_{56}$Ba	3.582 ± 0.290	3.040 ± 0.404	−17.829	3.077 ± 0.492	−16.412	3.076 ± 0.492	−16.450
	$_{57}$La	0.406 ± 0.042	0.296 ± 0.105	−37.162	0.299 ± 0.192	−35.786	0.299 ± 0.192	−35.786
143	$_{56}$Ba	2.851 ± 0.254	3.023 ± 0.349	5.690	2.886 ± 0.664	1.213	2.886 ± 0.664	1.213
	$_{57}$La	1.045 ± 0.109	0.822 ± 0.266	−27.129	0.815 ± 0.522	−28.221	0.815 ± 0.522	−28.221
144	$_{56}$Ba	2.679 ± 0.329	2.224 ± 0.321	−20.459	2.156 ± 0.690	−24.258	2.156 ± 0.690	−24.258
	$_{57}$La	1.228 ± 0.129	1.253 ± 0.311	1.995	1.309 ± 0.419	6.188	1.309 ± 0.419	6.188
145	$_{56}$Ba	0.824 ± 0.103	0.841 ± 0.212	2.021	0.803 ± 0.257	−2.615	0.803 ± 0.257	−2.615
	$_{57}$La	1.796 ± 0.365	1.722 ± 0.260	−4.297	1.697 ± 0.543	−5.834	1.697 ± 0.543	−5.834
	$_{58}$Ce	0.430 ± 0.055	0.451 ± 0.146	4.656	0.456 ± 0.292	5.702	0.456 ± 0.292	5.702
146	$_{56}$Ba	0.511 ± 0.057	0.248 ± 0.078	−106.048	0.238 ± 0.152	−114.706	0.238 ± 0.152	−114.706
	$_{57}$La	0.293 ± 0.028	0.449 ± 0.076	34.744	0.581 ± 0.372	49.570	0.415 ± 0.265	29.398
	$_{57}$La^{m}	0.742 ± 0.073	0.808 ± 0.137	8.168	0.581 ± 0.372	−27.711	0.747 ± 0.478	0.669
	$_{58}$Ce	0.793 ± 0.097	0.954 ± 0.206	16.876	1.038 ± 0.332	23.603	1.038 ± 0.332	23.603
147	$_{57}$La	0.655 ± 0.075	0.671 ± 0.161	2.385	0.611 ± 0.391	−7.201	0.610 ± 0.391	−7.377
	$_{58}$Ce	1.619 ± 0.178	1.190 ± 0.176	−36.050	1.216 ± 0.280	−33.141	1.216 ± 0.280	−33.141
148	$_{57}$La	0.191 ± 0.016	0.180 ± 0.060	−6.111	0.117 ± 0.075	−63.248	0.117 ± 0.075	−63.248
	$_{58}$Ce	0.920 ± 0.114	1.161 ± 0.123	20.758	0.890 ± 0.401	−3.371	0.890 ± 0.401	−3.371
151	$_{59}$Pr	0.419 ± 0.038	0.385 ± 0.068	−8.831	0.372 ± 0.238	−12.634	0.372 ± 0.238	−12.634
	$_{60}$Nd	0.289 ± 0.028	0.313 ± 0.065	7.668	0.292 ± 0.187	1.027	0.292 ± 0.187	1.027
152	$_{59}$Pr	0.028 ± 0.003	0.160 ± 0.045	82.500	0.160 ± 0.103	82.500	0.160 ± 0.103	82.500
	$_{60}$Nd	0.534 ± 0.066	0.393 ± 0.051	−35.878	0.370 ± 0.118	−44.324	0.370 ± 0.118	−44.324

(i) For the seven fission products, the sum of the isomeric- and ground-state yields obtained from our measurements is in good agreement with JEFF-3.1.1 within the error bars (at 1σ).

(ii) The ratio is also in good agreement with JEFF-3.1.1 for all fission products except for $^{98}_{39}$Y, where the R value is reversed between our data and JEFF-3.1.1, which is probably owing to a wrong assignment in the

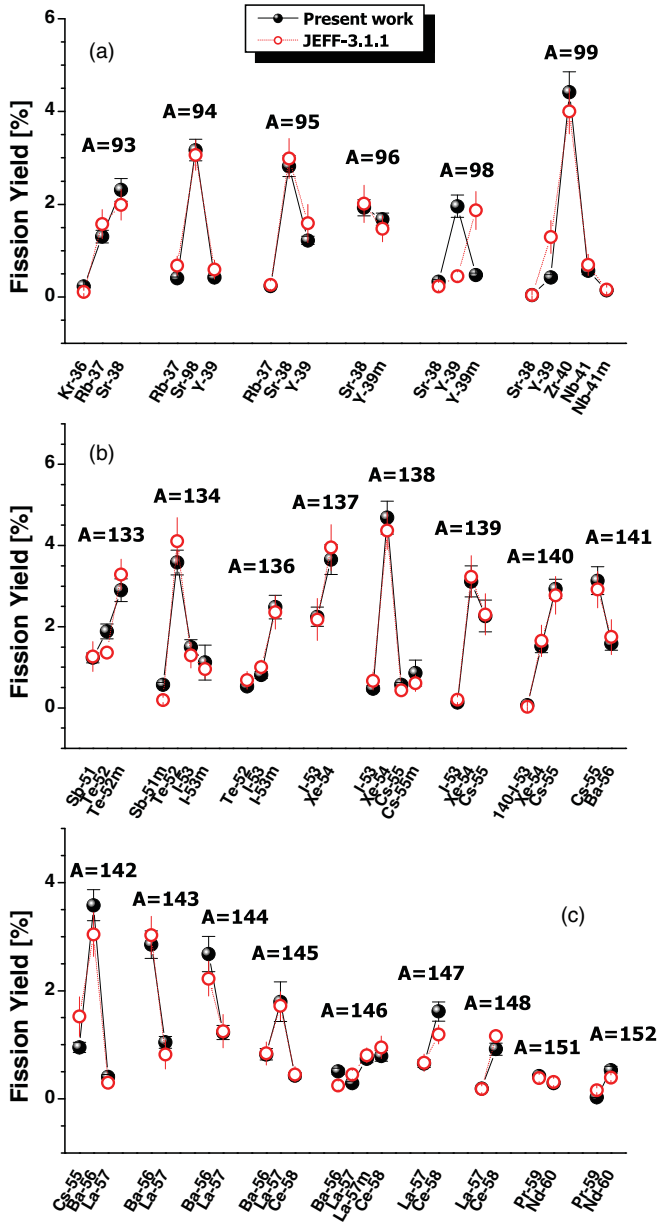

FIG. 8. (Color online) Isotopic yields measured in the present work and compared with JEFF-3.1.1 [5] in the light (a) and heavy (b, c) mass regions.

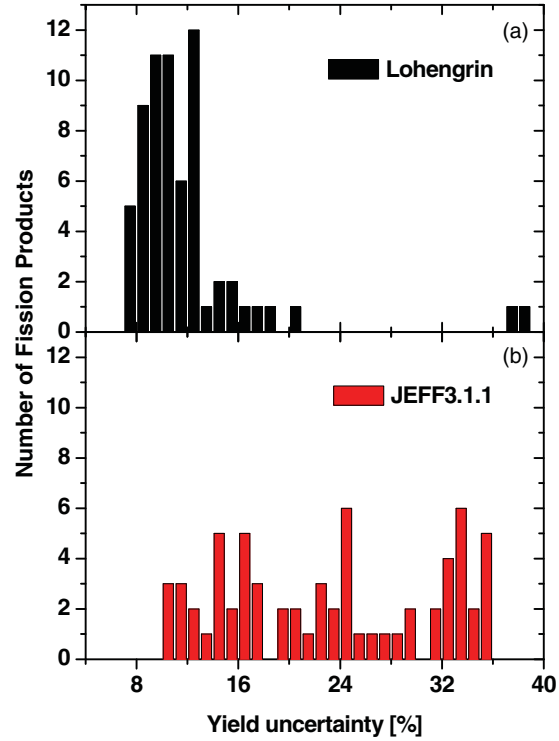

FIG. 9. (Color online) Histograms of the 65 fission product yield uncertainties for both our data (a) and JEFF-3.1.1 data (b).

European library between the isomeric and the ground state.

4. Nanosecond isomeric state

Some fission products show an asymmetric ionic charge distribution. In particular, an important tail for high ionic charge states can be observed. Such a distribution can not be explained by atomic considerations [37]. This effect, already observed in the past and explained by Wohlfarth [38], results from nanosecond isomers that decay by a highly converted internal transition. Owing to the short half-life of these isomeric states (of the order of some nanoseconds), conversion electrons, which are emitted between the target and the first dipole of the spectrometer, increase the ionic charge of the fission product. This new ionic charge state is maintained during the flight through Lohengrin and can therefore be detected. Unfortunately, because the isomeric decay has happened before the fission product arrives at the detection position, it is not possible to provide any spectroscopic information on the isomeric state, except a rough estimate of its half-life.

An example of such an isomeric state is given in Fig. 10. In this figure, the ionic charge distributions were measured by γ spectrometry for both $^{140}_{54}$Xe and $^{140}_{55}$Cs. A "normal" Gaussian shape was found for $^{140}_{54}$Xe (no nanosecond isomer), while for the $^{140}_{55}$Cs nucleus, a strong deformed distribution was observed, showing the presence of a nanosecond isomer. By this method, new nanosecond isomers for masses 137, 138, 140, 142, and 144 were identified and reported in detail by Materna *et al.* in Ref. [39].

5. Nuclear charge polarization

Isobaric charge distributions were investigated for all masses where at least three fission product yields were measured: $A = 94$, 95, 99 (light fission products) and $A = 134$, 138, 139, 142, 145, 146 (heavy fission products). Assuming a Gaussian shape distribution, the first moment [most probable charge: $Z_P(A)$] and the second moment [variance: $\sigma_Z(A)$] were determined (see Table VIII).

In low-energy fission, fission products present an average charge density different from the fissioning nucleus charge

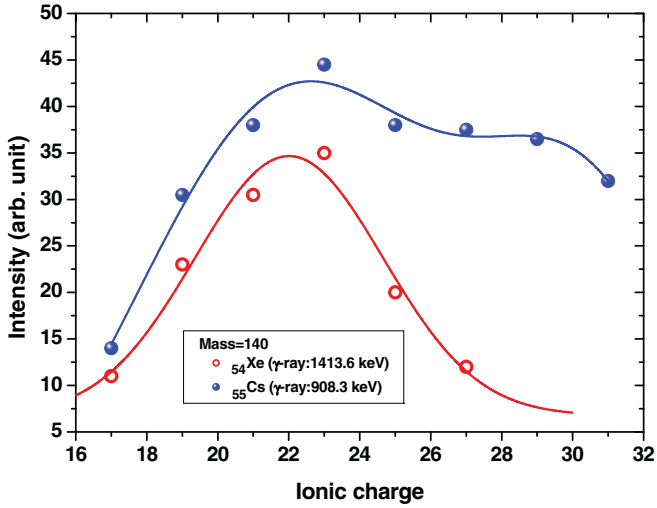

FIG. 10. (Color online) γ-ray intensity of $_{54}$Xe (1413.6 keV) and $_{55}$Cs (908.3 keV) for the mass 140 as a function of the ionic charge state. The Cs distribution clearly highlights a nanosecond isomeric state because of its asymmetric shape peaked on the high ionic charge states.

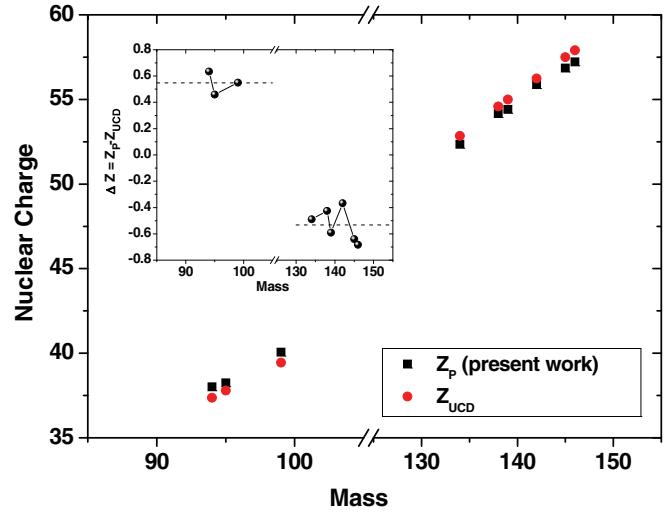

FIG. 11. (Color online) Most probable nuclear charge, Z_P, deduced from the present work and compared with $Z_{\rm UCD}$ calculated from Eq. (10). Inset: The difference $\Delta Z = Z_P - Z_{\rm UCD}$ as a function of mass. A clear nuclear charge polarization of about 0.5 unit can be observed.

density. This observation has been measured in a great number of experiments (see Refs. [40–42] and references therein). Compared to the unchanged charge density nuclear charge $Z_{\rm UCD}$, which is defined by Eq. (10), light fragments are found to have a smaller nuclear charge while heavy fragments show the opposite tendency:

$$Z_{\rm UCD}(A') = \frac{Z_F}{A_F}[A + \overline{\nu}(A')]. \qquad (10)$$

A represents the mass after prompt neutron emissions, while A' is the mass before prompt neutron emissions.

The difference ($\Delta Z = Z_P - Z_{\rm UCD}$) implies the existence of a charge polarization of nuclear matter. It is clearly apparent in Fig. 11 for the present ^{239}Pu($n_{\rm th}$, f) data, where $\overline{\nu}(A)$ values used in Eq. (10) come from evaluated data of Wahl [43]. The inset in Fig. 11 shows a consistent behavior of the average difference ($\langle\Delta Z\rangle$) between light and heavy mass regions. Indeed, we found 0.55 ± 0.05 and -0.53 ± 0.05, respectively, for light and heavy fission products. These values are in very good agreement with data from the literature (see, e.g., Ref. [42]). Besides, similar results were observed for close fissioning systems [40,41]. In addition to these remarks, results from K.-H. Schmidt [44] have revealed that the mean nuclear charge in the heavy mass region is centered around 54. The few ^{239}Pu($n_{\rm th}$, f) average nuclear charges reported in Table VIII seem to be in accordance with this observation.

TABLE VIII. Most probable (Z_P) and width (σ_Z) of nuclear charge distributions determined from the present measurements for various masses.

A	Z_P	σ_Z
94	38.0	0.5
95	38.2	0.5
99	40.1	0.5
134	52.4	0.7
138	54.2	0.5
139	54.4	0.5
142	55.9	0.5
145	56.9	0.7
146	57.2	1.0

C. Limitation of the method

As for all experiments based on γ spectrometry, the first main limitation is caused by the knowledge of decay data. Until now, despite many efforts made in γ-ray spectroscopy, a large number of nuclei (in particular, exotic nuclei) have not yet been measured with sufficient accuracy.

Another limitation for measuring isotopic yields by γ spectrometry is caused by the isotope lifetimes. Indeed, the isotopic yield determination of a long-living nucleus is experimentally too time-consuming. Thus, in general, yields can be measured only for isotopes with half-lives of less than a few hours, and of course, the γ spectrometry method completely rules out the investigation of stable nuclei.

Table IX summarizes the reasons why some isotopic yields could not be measured.

TABLE IX. Survey of the main reasons why some masses were not measured during our experimental campaign.

Mass	$T_{1/2}$ too long for at least one isotope	Nuclear decay data not well enough known	Yield too low
$\leqslant$132		X	
135	X		
149	X	X	
150	X	X	
$\geqslant$153			X

IV. CONCLUSION

Despite the insufficient knowledge of decay data, isotopic yield determination by γ-ray spectrometry has greatly improved yield measurements with the Lohengrin mass-spectrometer. Indeed, Lohengrin is today still the most accurate instrument for measuring thermal neutron fission yields, and with the present work, its range of application is practically doubled, now allowing also the study of isotopic yields of heavy fragments.

The experimental setup developed in the present work was shown to be a powerful tool for investigation of isotopic yields in all fission regions. Results presented in this work are very encouraging considering how uncertainties have been decreased compared to some other experiments and/or evaluated data.

Experimental campaigns are now starting to measure accurately the fission yields of various fissioning systems important for practical applications and for our knowledge of the fission process.

[1] J. Moreau and K. Heyde, in *The Nuclear Fission Process*, edited by C. Wagemans (CRC Press, Boca Raton, FL, 1991), p. 227.
[2] B. D. Wilkins *et al.*, Phys. Rev. C **14**, 1832 (1976).
[3] P. Möller *et al.*, Nature **409**, 785 (2001).
[4] H. Goutte, J. F. Berger, P. Casoli, and D. Gogny, Phys. Rev. C **71**, 024316 (2005).
[5] M. Kellett *et al.*, JEFF Report 20, NEA NØ6287 (OECD, 2009).
[6] M. B. Chadwick *et al.*, Nucl. Data Sheets **107**, 2931 (2006).
[7] K. Shibata *et al.*, J. Nucl. Sci. Technol. **48**, 1 (2011).
[8] H. O. Denschlag in *Experimental Techniques in Nuclear Physics*, edited by D.-N. Poenaru and W. Greiner (Berlin, 1997), p. 535.
[9] J. P. Bocquet *et al.*, Z. Phys. A **335**, 41 (1990).
[10] U. Quade *et al.*, Nucl. Phys. A **487**, 1 (1988).
[11] H. G. Clerc *et al.*, Nucl. Phys. A **247**, 74 (1975).
[12] G. Sieger *et al.*, Phys. Lett. B **53**, 45 (1974).
[13] J. L. Sida *et al.*, Nucl. Phys. A **502**, 233 (1989).
[14] G. Martinez *et al.*, Nucl. Phys. A **515**, 433 (1990).
[15] I. Tsekhanovich *et al.*, Nucl. Phys. A **688**, 633 (2001).
[16] C. Schmitt *et al.*, Nucl. Phys. A **430**, 21 (1984).
[17] T. Friedrichs, Ph.D. thesis, University of Brunswick, 1998.
[18] I. Tsekhanovich *et al.*, Nucl. Phys. A **658**, 217 (1999).
[19] D. Rochman *et al.*, Nucl. Phys. A **710**, 3 (2002).
[20] M. Djebara *et al.*, Nucl. Phys. A **496**, 346 (1989).
[21] D. Rochman, Ph.D. thesis, Strasbourg University, 2001.
[22] J. P. Bocquet *et al.*, Nucl. Instrum. Methods Phys. Res. A **267**, 466 (1988).
[23] E. Moll *et al.*, Nucl. Instrum. Methods **139**, 213 (1976).
[24] G. Fioni *et al.*, Nucl. Instrum. Methods A **332**, 175 (1993).
[25] H. Bateman, Proc. Cambridge Philos. Soc. **15**, 423–427 (1910).
[26] J. Theuerkauf *et al.*, *Program Tv*, unpublished (University of Cologne, Cologne, Germany).
[27] G. F. Knoll, in *Radiation Detection and Measurement*, 3rd ed. (John Wiley and Sons, New York, 1999), p. 448.
[28] U. Köster *et al.*, Nucl. Instrum. Methods A **613**, 363 (2010).
[29] J. Laurec *et al.*, Nucl. Data Sheets **111**, 2965 (2010).
[30] A. D. Belyaev *et al.*, Nucl. Instrum. Methods Phys. Res. Sec. B **43**, 5 (1989).
[31] A. Bail, Ph.D. thesis, University of Bordeaux, 2009.
[32] N. A. Gundorin *et al.*, in *Proceedings of the International Conference on Nuclear Data for Science and Technology, ND1994, Gatlinburg, Tennessee, May 9–13, 1994*, edited by J. K. Dickens (ANS, La Grange Park, IL, 1994), p. 139.
[33] A. A. Bogdzel *et al.*, in *Proceedings of the International Conference on Nuclear Data for Science and Technology, ND1991, Juelich (Germany), May 13–17, 1991*, edited by S. M. Qaim (Springer-Verlag, Berlin, 1991), p. 150.
[34] R. Brissot *et al.*, J. Phys. **37**, 241 (1976).
[35] S. J. Balestrini *et al.*, Phys. Rev. C **12**, 413 (1975).
[36] K. F. Flynn *et al.*, J. Inorg. Nucl. Chem. **37**, 869 (1975).
[37] Y. Baudinet-Robinet, Phys. Rev. A **26**, 62 (1982).
[38] H. Wohlfarth *et al.*, Z. Phys. A **287**, 153 (1978).
[39] T. Materna *et al.*, in *Proceedings of the International Workshop on Nuclear Fission and Fission Product Spectroscopy, Cadarache (France), May 13–16, 2009*, edited by A. Chatillon *et al.* (AIP Conference Proceedings, 2009), p. 367.
[40] H. Naik *et al.*, J. Phys. G **30**, 107 (2004).
[41] H. Naik *et al.*, Nucl. Phys. A **781**, 1 (2007).
[42] V. A. Roshchenko, V. M. Piksaikin, S. G. Isaev, and A. A. Goverdovski, Phys. Rev. C **74**, 014607 (2006).
[43] A. C. Wahl, At. Data Nucl. Data Tables **39**, 1 (1988).
[44] K. H. Schmidt *et al.*, Nucl. Phys. A **665**, 221 (2000).
[45] [http://www.nndc.bnl.gov].
[46] [http://ie.lbl.gov/toi.html].